Electronic Supplementary Material (ESI) for Journal of Materials Chemistry A.

Electronic Supporting Information (ESI)

Understanding the Efficient Electrocatalytic Activities of $MoSe_2$–Cu_2S Nanoheterostructures

Md. Samim Hassan,[a] Pooja Basera,[b] Soniya Gahlawat,[a] Pravin P. Ingole,[a] Saswata Bhattacharya,[b#] Sameer Sapra[a]*

[a]Department of Chemistry, Indian Institute of Technology Delhi, Hauz Khas, New Delhi 110016, India

[b]Department of Physics, Indian Institute of Technology Delhi, Hauz Khas, New Delhi 110016, India

*Email: sapra@chemistry.iitd.ac.in

#Email: saswata@physics.iitd.ac.in

Theoretical methodology:

The change in Gibbs free energy (ΔG) for each reaction step is evaluated based on calculated adsorption energies using the equation given below.

$$\Delta G_{ads} = \Delta E + \Delta ZPE - T\Delta S$$

Where, ΔE is defined as the difference between DFT free energies of without and with adsorbed intermediates *i.e.,* adsorption energy. ZPE is zero-point energy obtained from vibrational frequency calculations. ΔS is change in entropy obtained from standard tables for gas-phase molecules and T is temperature. The vibrational frequency calculations *i.e.* ZPE are obtained only for gas phase molecules and adsorbed species. However, ZPE is kept fixed for $MoSe_2$ NSs with periodic boundary conditions, by assuming that they encounter relatively minor vibrations. Note that, the entropies of the gas-phase molecules are taken from the NIST database, whereas the entropies are considered to be zero for all adsorbed species to the $MoSe_2$ NSs.

Absorbance spectra.

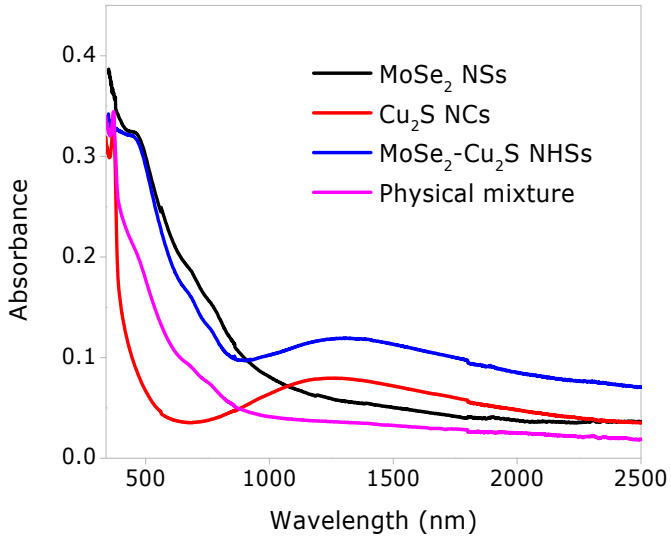

Fig. S1 Absorption spectra of pure $MoSe_2$ NSs, Cu_2S NCs, $MoSe_2$–Cu_2S NHSs, and corresponding physical mixtures.

For $MoSe_2$ NSs, the excitonic peaks are observed at 795 and 693 nm, which are well matches with the single monolayer morphology.[1,2] The Cu_2S NCs exhibit a short wavelength absorption edge below ~650 nm, attributed to the band edge absorption. The NCs also show absorbance in the NIR region owing to the presence of localized surface plasmons, which are derived from the oscillation of holes. In case of NHSs, along with the presence of $MoSe_2$ NSs feature, the NIR absorbance is red-shifted due to the delocalization of charge carriers. The red-shifting of surface plasmons is not observed in case of physical mixtures of these two constituents. Also in the physical mixtures, the surface plasmon is almost diminished. In physical mixtures, two components do not come in intimate contact. So in this case, the larger size of $MoSe_2$ shields the light to interact with the surface plasmon of Cu_2S. It might be a reason of diminishing the plasmonic feature. These studies indicate that the two counterparts come in an intimate contact only in case of NHSs.[3]

Raman spectra.

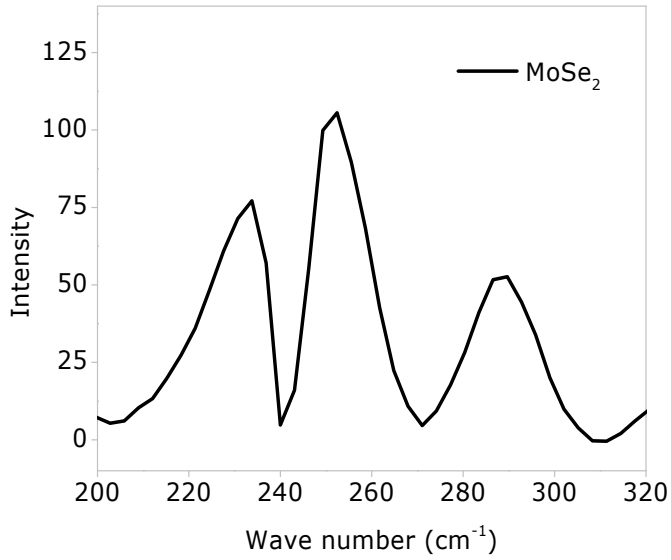

Fig. S2 Raman spectra of pure $MoSe_2$ NSs. The peak at ~252 cm^{-1} suggests the presence of Se vacancies in $MoSe_2$ NSs.

The presence of defects in $MoSe_2$ NSs is observed in Raman spectra. The two peaks ~ 232 and 287 cm^{-1} in $MoSe_2$ NSs correspond to the A_{1g}, and E_{2g} transitions, respectively. The presence of peak at 252 cm^{-1} is the signature defect peak that shows the presence of large number of selenium vacancies in the NSs.[4] These vacancies act as center for the growth of NHSs via passivating defects with thiol molecules.

TEM images.

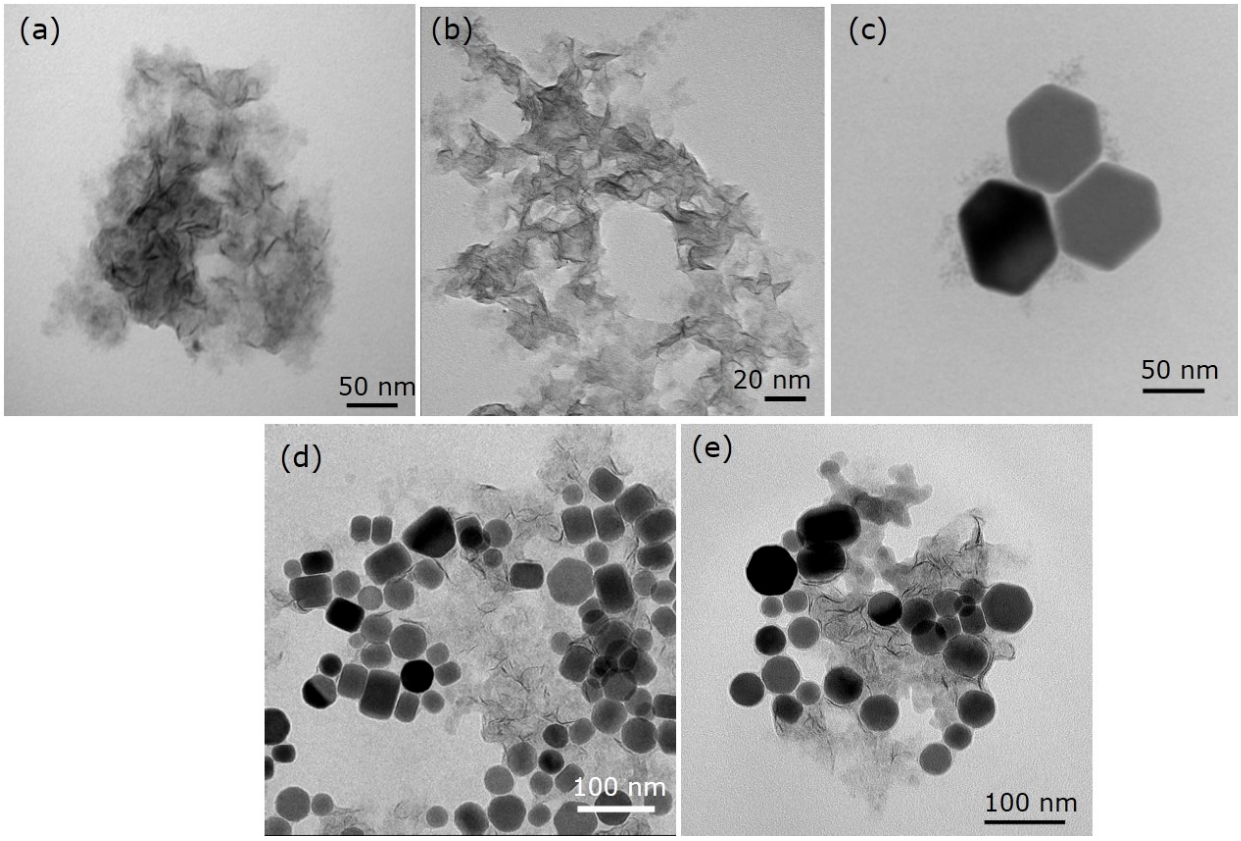

Fig. S3 TEM images of $MoSe_2$ (a) 50 nm and (b) 20 nm scale bar; (c) Cu_2S NCs; (d) and (e) $MoSe_2$−Cu_2S NHSs in different scale bar, showing the distribution of Cu_2S NCs over the basal planes of $MoSe_2$ NSs. In NHSs, these two entities are not separated even upon repeated washing and sonication, implying the formation of an intimate contact between these two constituent materials.

BET analysis.

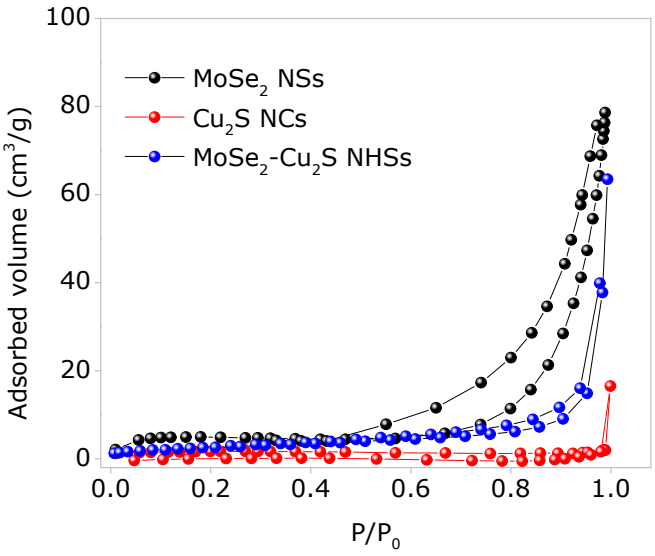

Fig. S4 N_2 adsorption-desorption isotherms of the materials. This indicates that the surface area of Cu_2S NCs is much lower as compared to $MoSe_2$ NSs, whereas the surface area of NHHs is comparable to that of $MoSe_2$ NSs.

Projected Density of states (PDOS).

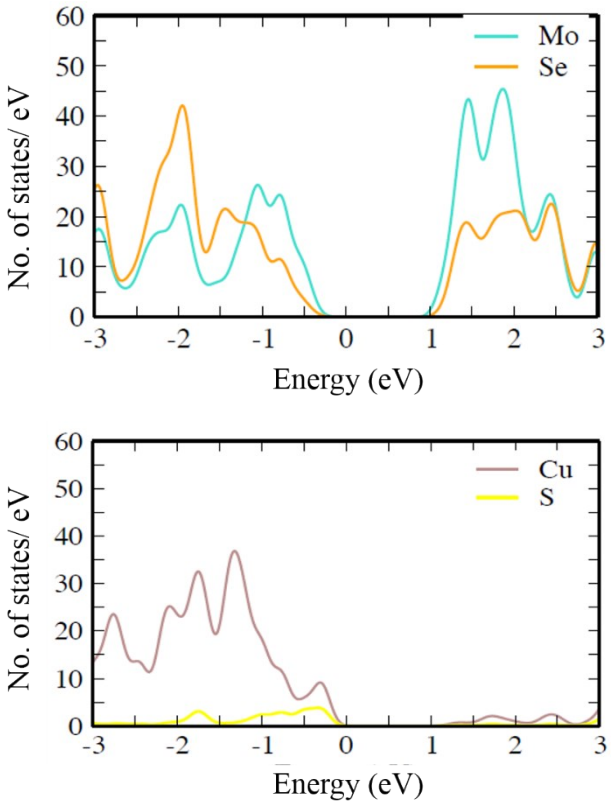

Fig. S5 Projected density of states (PDOS) of $MoSe_2$−Cu_2S NHSs shows the contribution of each atoms.

From **Fig. S5** we have observed that, Mo atom has significant contribution in conduction band, whereas at valence band Se atom has enlarged contribution. In case of Cu_2S, Cu atom is primarily contributed at valence band as well as conduction band. On comparing both the Figure, it is observed that Cu atom is contributed primarily at valence band maximum near Fermi-level. However, Mo atom is majorly contributed near conduction band minimum near Fermi-level. This leads to form type-II heterojunction at the interfaces.

Table S1. Performance comparison of $MoSe_2$–Cu_2S NHSs toward OER with the reported materials in the literature

Reference	Electrocatalyst	$\eta@J = 10\ mA/cm^2$ (mA/cm^2) mV	Tafel slope (mV/decade)
This work	$MoSe_2$–Cu_2S NHSs	**264**	**63**
Chem. Mater. 2019, 31, 18, 7732–7743	Cu_2S	380	96
Angew. Chem. Int. Ed. 2020, 59, 21106 –21113	CoFe Oxide @ 2D Black Phosphorus	266	42
Chem. Mater. 2019, 10.1021/acs.chemmater.0c03543	Ni2P@NSG (nitrogen, sulfur doped grapheme) heterostructure	274	43
ACS Nano 2018, 12, 5297−5305	$NiPS_3$ nanosheet - graphene composites	294	42.6
Angew. Chem. Int. Ed. 2020, 59, 11948 – 11957	$Co_2Mo_3O_8$@NC (N rich carbon layer)	331	87.5
ACS Appl. Mater. Interfaces 2018, 10, 35025−35038	Nickel/Molybdenum Carbide-Anchored N‑Doped Graphene/CNT Hybrid	328	74
ChemSusChem 2020, 13, 1–9	CuSe	297	89
J. Mater. Chem. A, 2020, 8, 3083	CdS@Co_9S_8/Ni_3S_2	285	108.5
ACS Catal. 2018, 8, 1683−1689	MoS_2 quantum dots	370	39
Adv. Funct. Mater. 2017, 27, 1702300	Mo–N/C@MoS_2	390	72

Catal. Sci. Technol., 2019, 9, 406	Ni-Doped CuS	390	96.8
Angew. Chem. Int. Ed. 2016, 55, 6702–6707	MoS_2/Ni_3S_2	218	88

EIS measurement in open circuit and thermodynamic potential.

When an electrode is dipped into an electrolyte solution, then a potential is generated at their interfaces, which is called as 'open circuit potential' (OCP). At OCP, the whole electrochemical system is stable. At potential higher than OCP, surface of electrode is modified. At OCP, one can measure the intrinsic catalytic properties of material without any surface modification. On the other hand, thermodynamic potential is the standard potential, where ideally a Faradaic process is started. For OER, the potential value is 1.23 V vs RHE. However, in practical this process requires greater potential to overcome the energy barriers, called as overpotential (η). The deviation is originating mainly from the kinetic barrier of reaction and partly from internal resistance of solvent, electrocatalyst, contact resistance of wires, electrochemical workstation, and the electrodes.

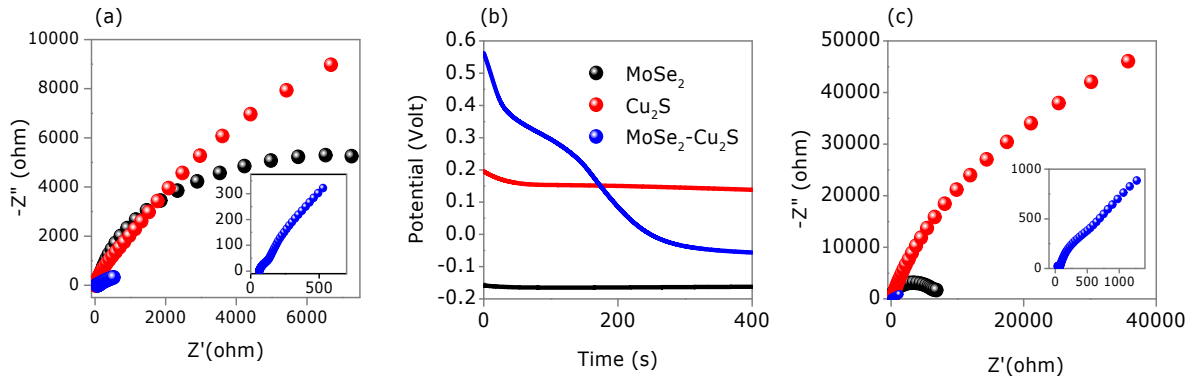

Fig. S6 (a) EIS spectra of the electrocatalysts collected at the thermodynamic potential; (b)

open circuit potential (OCP) measurements; (c) EIS spectra collected at the OCP for individual catalysts.

From these analysis it is observed that in case of $MoSe_2$−Cu_2S NHSs, the charge transfer resistance value is much lower at thermodynamic as well as at open circuit potential, as compared to their individual counterparts. It manifest that the intrinsic charge transfer resistance of $MoSe_2$-Cu_2S NHSs is much lower as compared to the $MoSe_2$ NSs and Cu_2S NCs.

ECSA measurement.

Double layer capacitance is calculated using Randles Sevcik equation. In non-faradaic region, a minute current is flowed due to the surface adsorption-desorption phenomenon. In this case at the interfaces of electrode-electrolyte, a capacitance is generated in the form of double layers. The linear fitting of the difference of peak current density ($J_{pc} - J_{pa}$) against the respective scan rate (**Fig. 4d**) provides information about the double layer capacitance (C_{dl}). This C_{dl} value is related to the number of active sites present in the electrocatalyst. The higher value of C_{dl} suggests more amount of electrolyte comes into the contact of electrodes, which in other words gives information about the number of catalytic centers *i.e.* electrochemical surface area.[5]

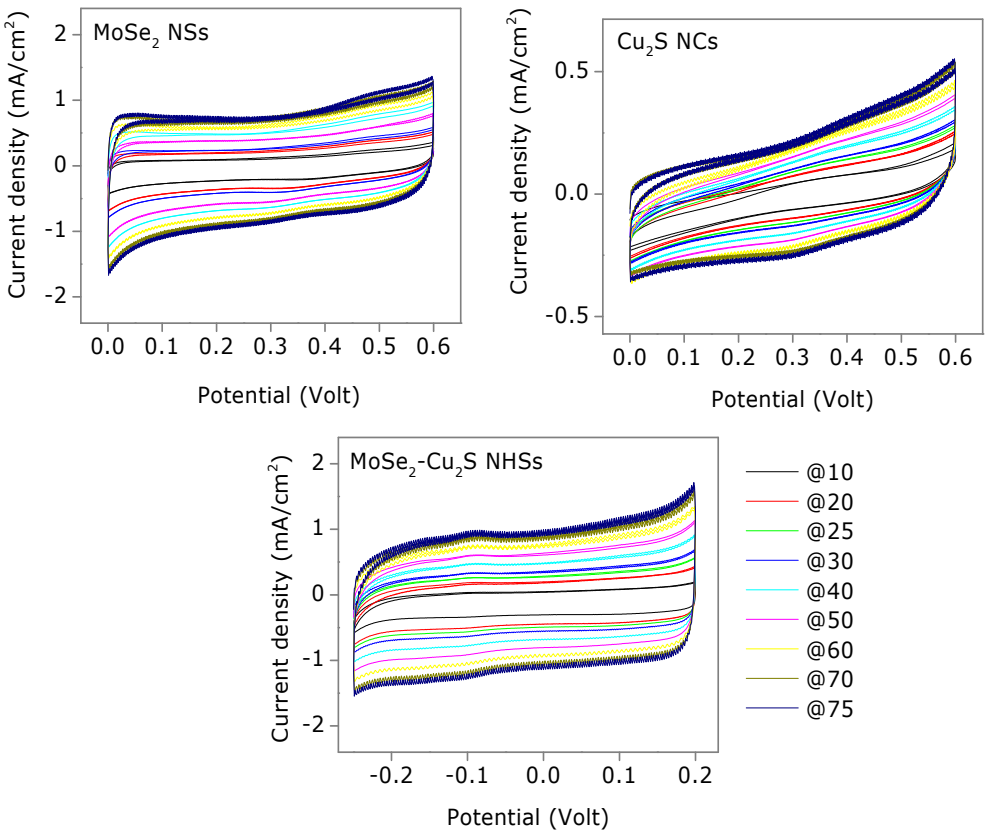

Fig. S7 Cyclic voltammogram of the electrocatalysts at different scan rates (10, 20, 25, 40, 50, 70 and 75 mV/s).

From the cyclic voltammogram plot, double layer capacitances (C_{dl}) for individual electrocatalysts are obtained.[6] From these value the electrochemical surface area is estimated as 109.4 cm^2, 33.2 cm^2, and 186.3 cm^2 for $MoSe_2$ NSs, Cu_2S NCs and $MoSe_2$-Cu_2S NHSs, respectively. The electrochemically active surface area can be calculated from the following equation

$$ECSA = \frac{specific\ capacitance}{40\ \mu F\ cm^{-2}/\ cm^2_{ECSA}}$$

Intrinsic catalytic activity of catalysts.

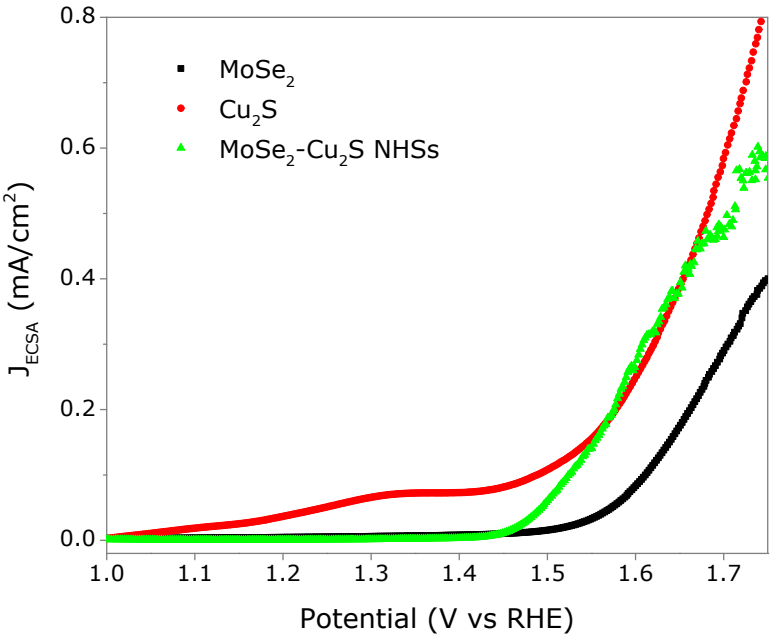

Fig. S8 Polarization curves with current density **(Fig. 4a)** normalized by electrochemically active surface area (ECSA). This plot provides the information about the intrinsic catalytic activity of the materials in terms of number of active sites.

XPS spectra of post-electrocatalytic $MoSe_2$−Cu_2S NHSs

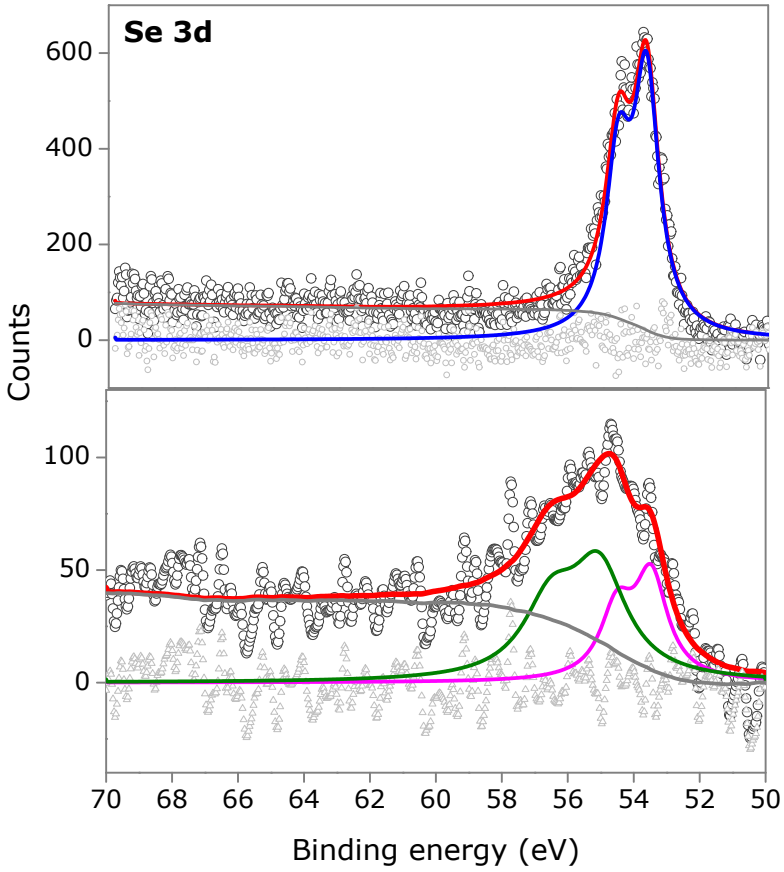

Fig. S9 Se 3d region of XPS spectra of $MoSe_2$−Cu_2S NHSs before and after 200 CV cycles.

Se 3d survey of post-electrocatalytic NHSs shows that the narrow features ~54 eV is broadened, confirming the presence of more than one species in this region. In the deconvoluted Se 3d spectrum, two set of doublets are observed, one at 53.5 ($^{3d_{5/2}}$) and 54.4 eV ($^{3d_{3/2}}$), whereas the other one is observed at 55.2 ($^{3d_{5/2}}$) and 56.5 eV ($^{3d_{3/2}}$). The former one can be assigned to Se (-II), whereas the latter one is attributed to the oxidized Se, which is formed during OER.

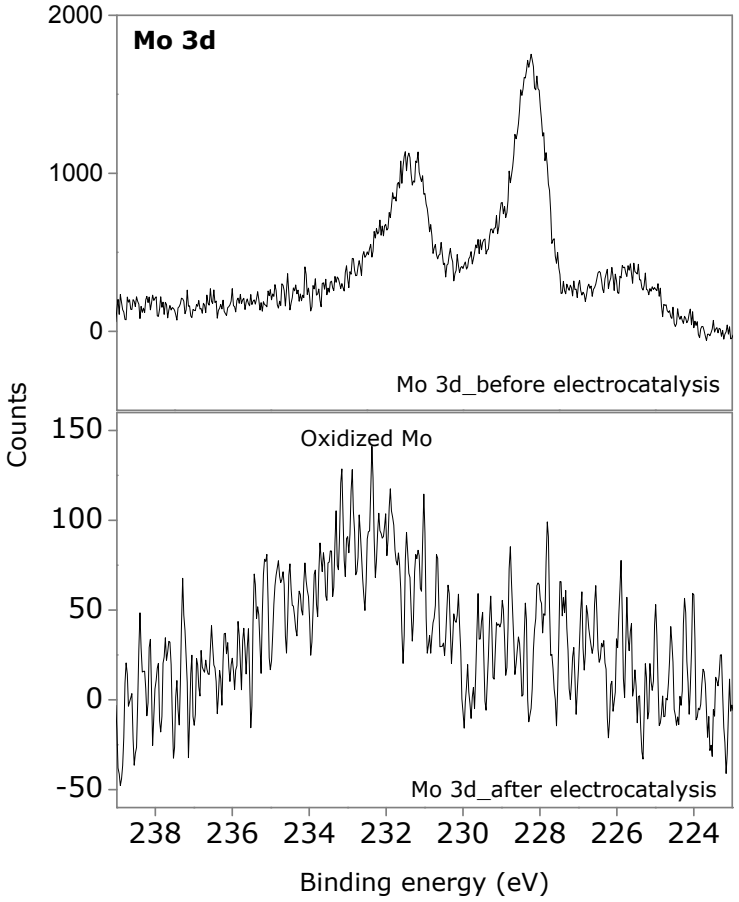

Fig. S10 Mo 3d region of XPS spectra of $MoSe_2$−Cu_2S NHSs before and after 200 CV cycles.

The spectra shows that the Mo (IV) peak are shifted towards high BEs, corresponding to the oxidation of Mo (IV) into Mo (VI). This also concluded that the oxidation is occurred at Mo during OER.[7] Cui and co-workers showed that the oxidized Mo in MoO_2 is helpful to improve the OER activity.[8]

CV cycle of post-electrocatalytic $MoSe_2$−Cu_2S NHSs

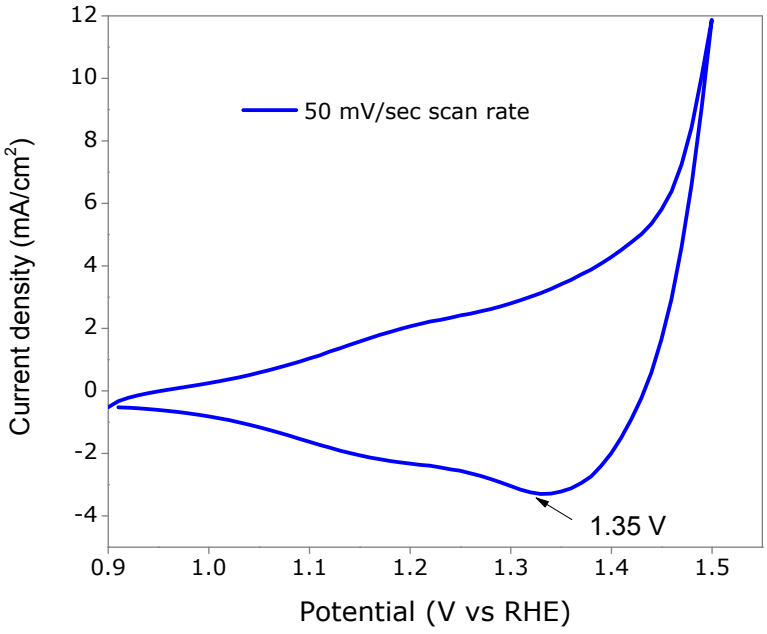

Fig. S11 Polarization CV of $MoSe_2$−Cu_2S NHSs collected at 50 mV/s scan rate after 200 CV cycles.

The cathodic peak at 1.35 V obtained on the OER curve of $MoSe_2$−Cu_2S NHSs is attributed to the reduction of Cu^{3+} to Cu^{2+}. In anodic potential, the peak corresponds to Cu^{2+} to Cu^{3+} is not observed, as it may overlap with the high current density in the anodic potential.[9]

TEM images after 200 CV cycles.

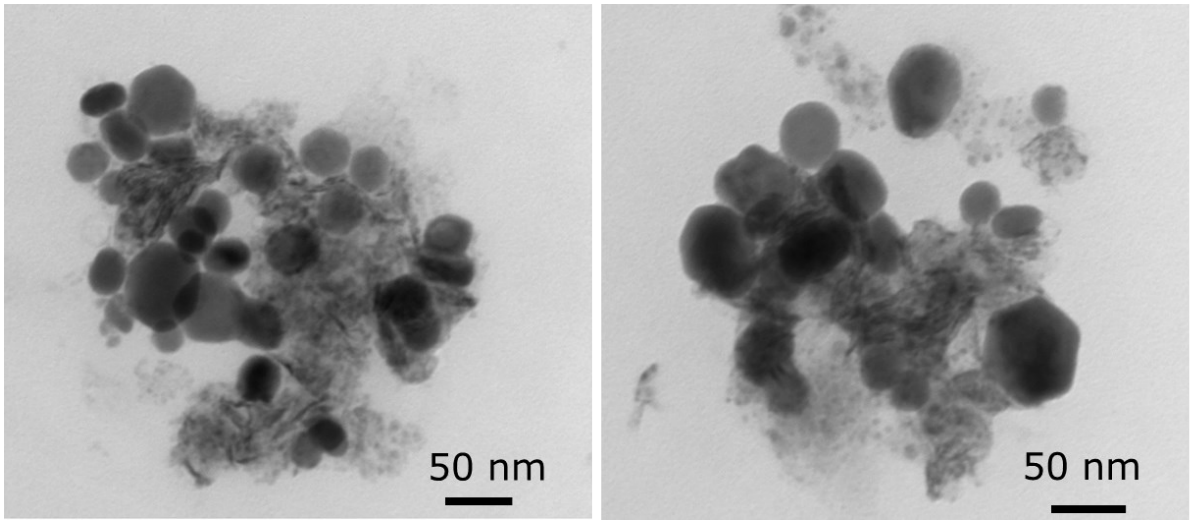

Fig. S12 TEM images of $MoSe_2$−Cu_2S NHSs after 200 CV cycles.

Characterizations of $MoSe_2$−Cu_2S NHSs after Chronoamperometry.

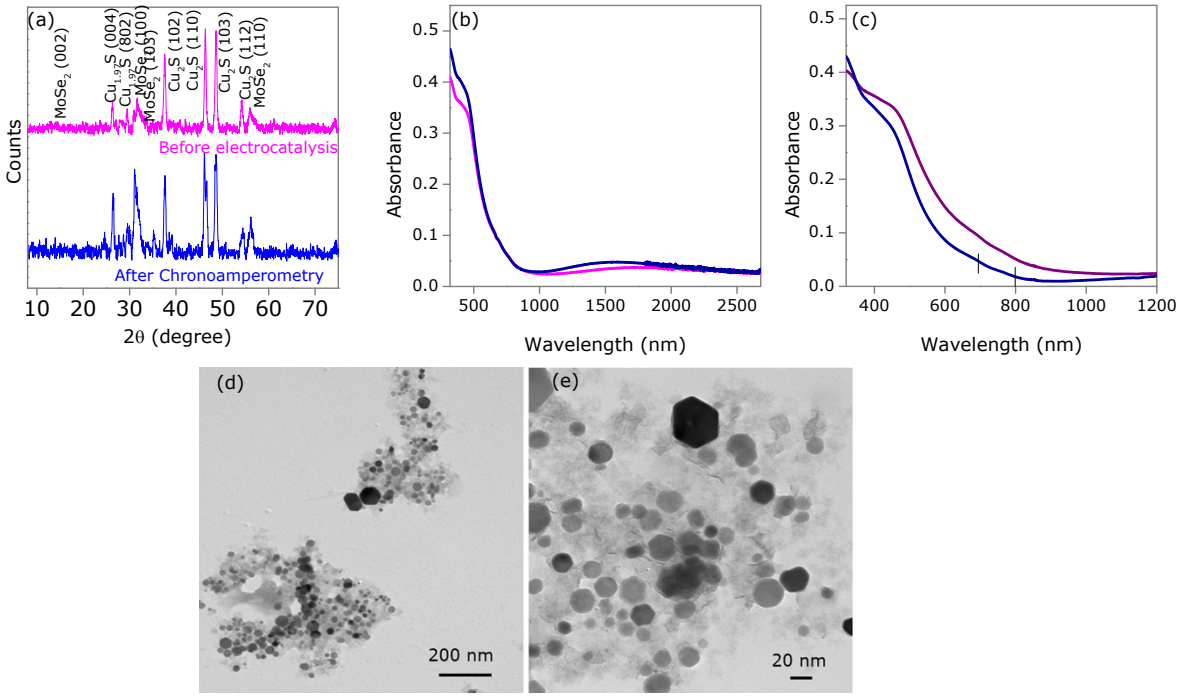

Fig. S13 (a) PXRD pattern; (b) absorbance spectra in wider wavelength and (c) lower wavelength region of $MoSe_2$-Cu_2S NHSs before and after chronoamperometry; TEM images of $MoSe_2$-Cu_2S NHSs after chronoamperometry (d) 200 nm and (e) 20 nm scale bar.

PXRD pattern indicates that after chronoamperometry there is co-existence of $MoSe_2$, Cu_2S, and $Cu_{1.97}S$ in NHSs, having no impurities of other species. This indicates that the crystal structure is retained after chronoamperometry. The only noticeable change we observed that the intensity corresponds to $Cu_{1.97}S$ is increased, owing to the surface oxidation of Cu (I). Absorbance spectra suggests that after chronoamperometry both the features of $MoSe_2$ NSs and Cu_2S NCs are retained in $MoSe_2$-Cu_2S NHSs. It is observed that the surface plasmon intensity in the NIR region is increased due to increase the contents of Cu (II) species, which is formed during catalysis.[10] TEM studies indicate that the morphology of the $MoSe_2$–Cu_2S NHSs is retained after

chronoamperometry *i.e.* Cu_2S NCs is decorated at the basal planes of $MoSe_2$ NSs in NHSs. All these studies suggest that the core of NHSs is preserved after chronoamperometry.

OER Reaction mechanism of Cu_2S NCs.

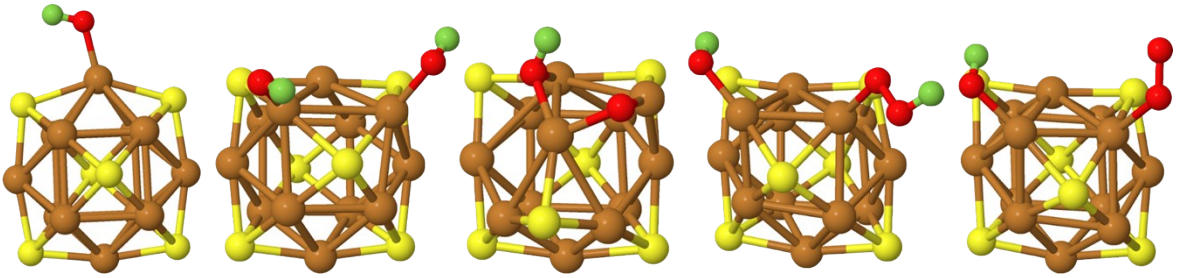

Fig. S14 Relaxed structures shown for Cu_2S NCs for OER activity.

OER Reaction mechanism of $MoSe_2$ NSs.

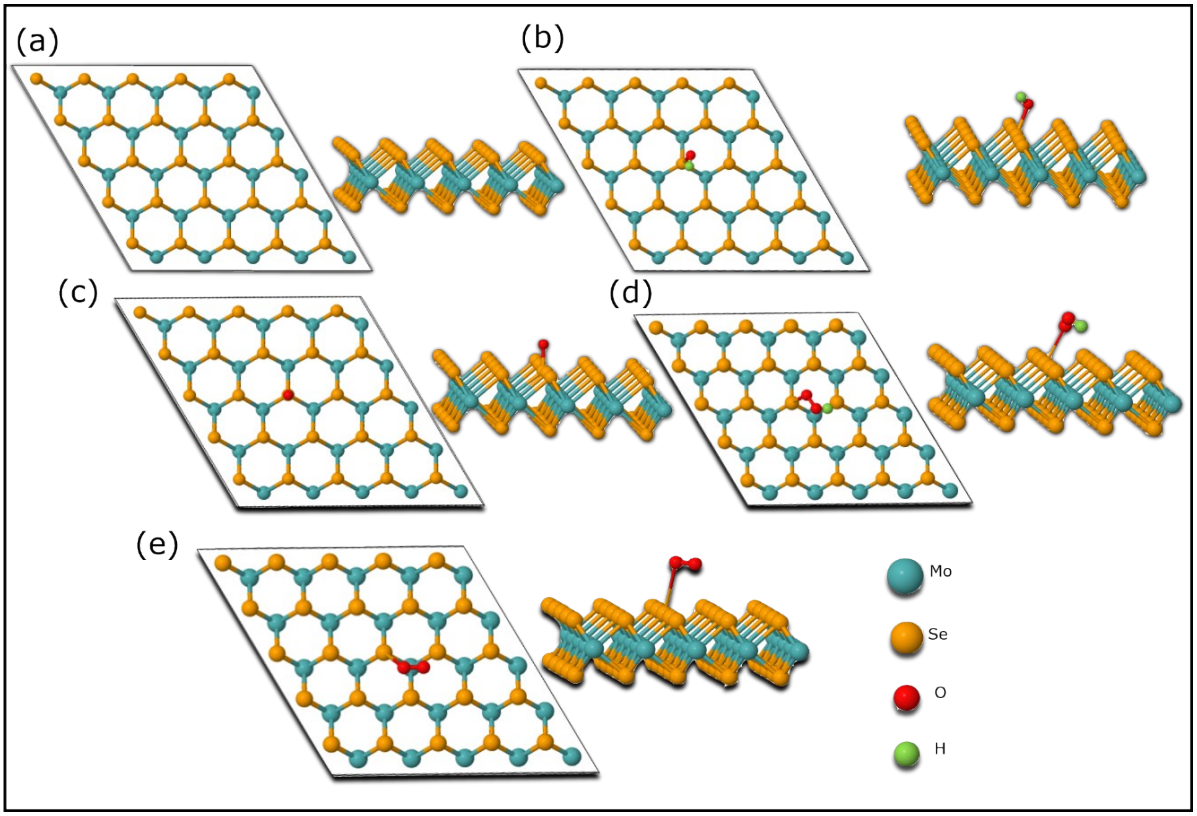

Fig. S15 Top and side view of relaxed structures shown for $MoSe_2$ NSs for OER activity.

HER activity in acidic medium.

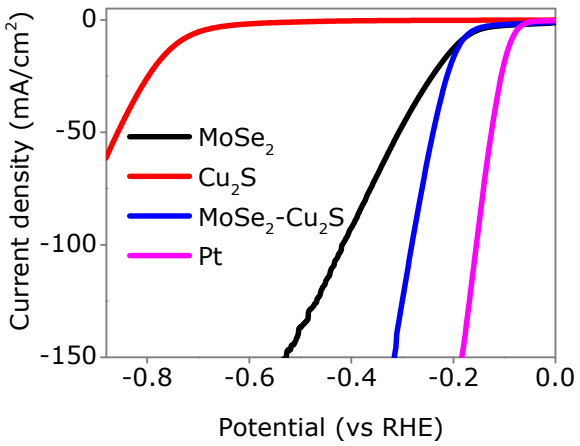

Fig. S16 LSV plots of $MoSe_2$ NSs, Cu_2S NCs, $MoSe_2$–Cu_2S NHSs and Pt toward HER activity in acidic medium.

EIS measurement in alkaline medium.

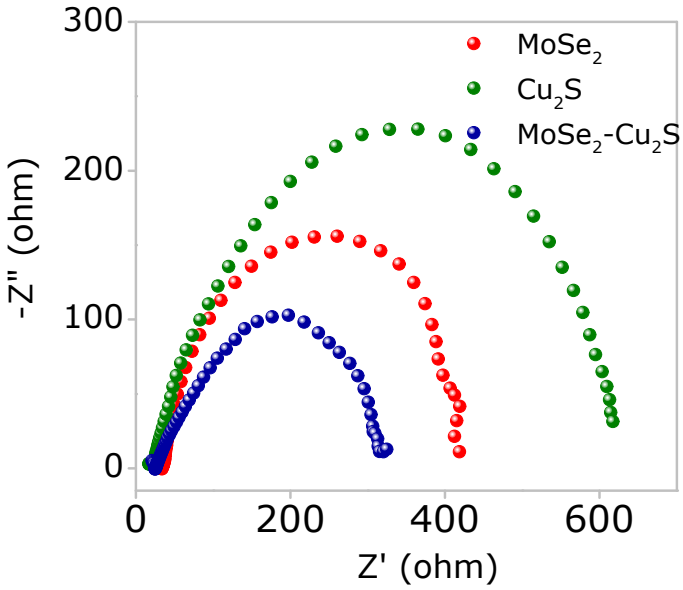

Fig. S17 Nyquist plots of $MoSe_2$ NSs, Cu_2S NCs and $MoSe_2$–Cu_2S NHSs in alkaline medium for electrocatalytic HER. This indicates that NHSs possess lower charge transfer resistance as compared to their pure counterparts.

References.

1 W. Jung, S. Lee, D. Yoo, S. Jeong, P. Miró, A. Kuc, T. Heine and J. Cheon, *J. Am. Chem. Soc.*, 2015, **137**, 7266–7269.

2 M. S. Hassan, A. Jana, S. Gahlawat, N. Bhandary, S. Bera, P. P. Ingole and S. Sapra, *Bull. Mater. Sci.*, 2019, **42**, 74.

3 M. S. Hassan, S. Bera, D. Gupta, S. K. Ray and S. Sapra, *ACS Appl. Mater. Interfaces*, 2019, **11**, 4074–4083.

4 M. Mahjouri-Samani, L. Liang, A. Oyedele, Y.-S. Kim, M. Tian, N. Cross, K. Wang, M.-W. Lin, A. Boulesbaa, C. M. Rouleau, A. A. Puretzky, K. Xiao, M. Yoon, G. Eres, G. Duscher, B. G. Sumpter and D. B. Geohegan, *Nano Lett.*, 2016, **16**, 5213–5220.

5 Q. Liang, L. Zhong, C. Du, Y. Luo, J. Zhao, Y. Zheng, J. Xu, J. Ma, C. Liu, S. Li and Q. Yan, *ACS Nano*, 2019, **13**, 7975–7984.

6 W. Yuan, S. Wang, Y. Ma, Y. Qiu, Y. An and L. Cheng, *ACS Energy Lett.*, 2020, **5**, 692–700.

7 D. Das, S. Santra and K. K. Nanda, *ACS Appl. Mater. Interfaces*, 2018, **10**, 35025–35038.

8 Y. Jin, H. Wang, J. Li, X. Yue, Y. Han, P. K. Shen and Y. Cui, *Adv. Mater.*, 2016, **28**, 3785–3790.

9 Y. Zuo, Y. Liu, J. Li, R. Du, X. Han, T. Zhang, J. Arbiol, N. J. Divins, J. Llorca, N. Guijarro, K. Sivula and A. Cabot, *Chem. Mater.*, 2019, **31**, 7732–7743.

10 Y. Zhao, H. Pan, Y. Lou, X. Qiu, J. Zhu and C. Burda, *J. Am. Chem. Soc.*, 2009, **131**, 4253–4261.